Available online at www.eccomasproceedia.org
Eccomas Proceedia COMPDYN (2019) 5291-5303

ECCOMAS
Proceedia

COMPDYN 2019
7th ECCOMAS Thematic Conference on
Computational Methods in Structural Dynamics and Earthquake Engineering
M. Papadrakakis, M. Fragiadakis (eds.)
Crete, Greece, 24–26 June 2019

ACCURATE AND EFFICIENT MODELING OF THE HYSTERETIC BEHAVIOR OF SLIDING BEARINGS

N. Vaiana, S. Sessa, M. Paradiso and L. Rosati

Department of Structures for Engineering and Architecture, University of Naples Federico II
Via Claudio, 21, 80124 Naples, Italy
e-mail: nicolovaiana@outlook.it

Abstract. *This paper presents a uniaxial phenomenological model for the simulation of the hysteretic behavior typically exhibited by sliding bearings deforming along one of their transverse directions under the effect of an axial compressive load. The proposed hysteretic model is able to take into account the dependency of the device restoring force on the velocity of sliding, on the bearing pressure, and on the condition of the sliding interface. Furthermore, it allows for a considerable reduction of the computational effort of nonlinear dynamic analyses since the model hysteretic variable is evaluated by solving an algebraic equation. The numerical accuracy and computational efficiency of the proposed model are assessed by means of numerical simulations.*

Keywords: Sliding Bearing, Hysteretic Behavior, Phenomenological Model.

ISSN:2623-3347
Peer-review under responsibility of the organizing committee of COMPDYN 2019.
doi: 10.7712/120119.7304.19506

1 INTRODUCTION

Base isolation represents one of the most effective techniques for the seismic protection of buildings and bridges [1, 2, 3]. Such a technique requires the use of special devices, called seismic isolation bearings, having flexibility and energy dissipation capacity along their transverse directions and a large axial stiffness [4, 5].

Seismic isolation bearings can be divided into two main categories, that is, elastomeric and sliding bearings. The latter, of particular interest in this work, are devices made up of rigid plates that can slide with respect to each other. Looking at the type of sliding surface, it is possible to distinguish between flat surface sliding bearings and curved surface sliding bearings [6].

Sliding bearings deforming along one of their transverse directions under the effect of an axial compressive load display a hysteretic behavior due to the friction occurring at the sliding interface. Experimental tests results available in the literature show that the device restoring force depends not only on the device transverse displacement but also on the device transverse velocity. In particular, the dependency of the device restoring force on the velocity of sliding is due to the variation of the kinetic friction coefficient with the sliding velocity [7, 8].

Several hysteretic models have been proposed in the literature for simulating the complex behavior occurring in sliding bearings [9]. Among existing models, the one proposed by Mokha et al. [10] seems to be the most suitable one since it allows for an accurate prediction of the hysteretic response of both flat and curved surface sliding bearings by using a relatively small number of parameters. In particular, such a model is able to take into account the dependency of the restoring force on the velocity of sliding, on the bearing pressure, and on the condition of the sliding interface. Unfortunately, this model is not computationally efficient since it requires the numerical solution of a first-order nonlinear ordinary differential equation for the evaluation of the hysteretic variable at each time step of a nonlinear dynamic analysis.

This paper presents a uniaxial phenomenological model able to predict the hysteretic behavior generally displayed by sliding bearings. Compared to the model formulated by Mokha et al. [10], the proposed one not only offers the important advantage of accurately simulating the response of such devices, but it also allows for a considerable reduction of the computational effort required by nonlinear dynamic analyses since the model hysteretic variable is evaluated by solving an algebraic equation. Furthermore, it is based on a smaller set of parameters and can be easily implemented in a computer program.

2 SLIDING BEARINGS

Sliding bearings are seismic isolation devices consisting of a slider that moves on a sliding surface. Such devices, having an axial stiffness that is very much greater than the transverse one, display an energy dissipation capacity due to the friction damping occurring at the sliding interface [4].

According to the type of sliding surface, sliding bearings can be classified into two main categories, namely, Flat Surface Sliding Bearings (FSSBs) and Curved Surface Sliding Bearings (CSSBs) [6].

In this section, the main characteristics of the two above-mentioned types of sliding bearings are illustrated with particular emphasis on the brief description of the hysteretic behavior displayed along their transverse directions under the effect of an axial compressive load.

2.1 Flat Surface Sliding Bearings

Figure 1a shows the sectional view of a typical FSSB in deformed configuration. Such a device has a slider generally made up of an upper sliding plate and a lower polished stainless steel plate. The flat sliding surface is typically overlain by unfilled or filled Polytetrafluoroethylene, referred to as PTFE or Teflon.

FSSBs deforming along one of their transverse directions under the effect an axial compressive load display both rate-dependent and rate-independent hysteretic behaviors. Indeed, experimental test results available in the literature [7, 8] show that the device restoring force f depends not only on the device transverse displacement u but also on the device transverse velocity $\dot{u}$. Figure 1b shows the typical hysteresis loop shape displayed by FSSBs.

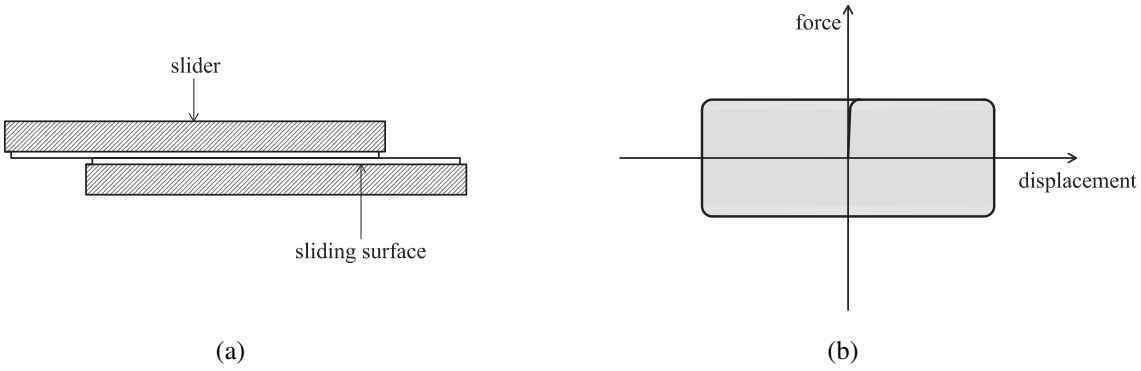

Figure 1: Typical FSSB: sectional view in deformed configuration (a) and hysteresis loop shape (b).

2.2 Curved Surface Sliding Bearings

Figure 2a shows the sectional view of a typical CSSB in deformed configuration. Such a device, denominated Friction Pendulum Bearing (FPB), has an articulated slider generally coated with a low-friction and high-pressure capacity composite material, typically PTFE. The curved sliding surface, having radius of curvature R, is generally overlain by polished stainless steel.

FPBs deforming along one of their transverse directions under the effect an axial compressive load display both rate-dependent and rate-independent hysteretic behaviors. Figure 2b shows the typical hysteresis loop shape displayed by FPBs.

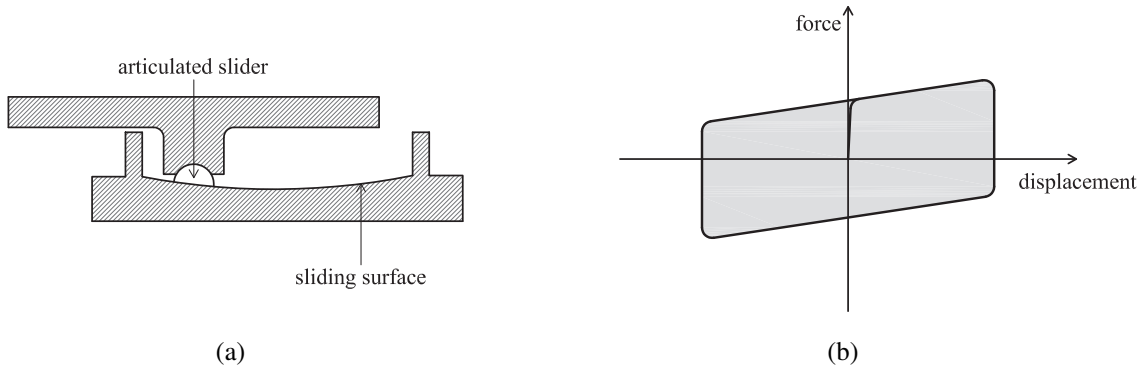

Figure 2: Typical FPB: sectional view in deformed configuration (a) and hysteresis loop shape (b).

3 PROPOSED HYSTERETIC MODEL

In this section, we first present the proposed hysteretic model formulation; subsequently, we illustrate a schematic flowchart of the model to allow for an easy computer implementation.

3.1 Model Formulation

The restoring force of a sliding bearing may be evaluated as [10]:

$$f\left(u,\dot{u}\right)=\frac{N}{R}u+\mu\left(\dot{u}\right)Nz\left(u\right), \tag{1}$$

where N is the axial compressive force acting on the bearing, R is the radius of curvature of the sliding surface, $\mu\left(\dot{u}\right)$ is the kinetic coefficient of friction, $z(u)$ is a dimensionless hysteretic variable, whereas u and $\dot{u}$ are the bearing transverse displacement and velocity, respectively.

The kinetic friction coefficient $\mu\left(\dot{u}\right)$ may be computed as [8]:

$$\mu\left(\dot{u}\right)=\mu_{max}-\left(\mu_{max}-\mu_{min}\right)e^{-a|\dot{u}|}, \tag{2}$$

where μ_{max} (μ_{min}) is the value of the kinetic friction coefficient at large (low) bearing transverse velocity, and a is a parameter, having units of time per unit length, that rules the velocity of transition of $\mu\left(\dot{u}\right)$ from μ_{min} to μ_{max}. Note that the values of μ_{max}, μ_{min}, and a depend on the bearing pressure, temperature, as well as condition of the sliding surface.

The dimensionless hysteretic variable $z(u)$ is a function of u and has a unit maximum absolute value, that is, $max\left\{|z(u)|\right\}=1$; in particular, if u cycles between two values, $z(u)$ traces a hysteresis loop bounded by two parallel horizontal straight lines.

In the model proposed by Mokha et al. [10], such a variable is evaluated by solving the following differential equation, typical of the celebrated Bouc-Wen model [11, 12]:

$$Y\dot{z}+\gamma\left|\dot{u}\right|z\left|z\right|^{n-1}+\beta\dot{u}\left|z\right|^{n}-A\dot{u}=0, \tag{3}$$

where $Y>0$ is a parameter having dimension of displacement, whereas A, β, γ, and n are dimensionless parameters. Unfortunately, the numerical solution of Equation (3) for each time step of a nonlinear dynamic analysis may significantly increase the overall computational effort.

To decrease the computational burden of the analyses without decreasing the accuracy of the numerical results, we propose to evaluate $z(u)$ by employing a specific instance of the general class of uniaxial phenomenological models formulated by Vaiana et al. [13, 14].

According to such a general formulation, a generic hysteresis loop, in the z-u plane, can be described by means of four types of curves, that is, the upper c_u and the lower c_l limiting curves and the generic loading c^+ and unloading c^- curves.

As shown in Figure 3, the upper (lower) limiting curve c_u (c_l) intercepts the vertical axis at $z=\bar{f}$ ($z=-\bar{f}$). Furthermore, the generic loading (unloading) curve has a starting point, lying on the lower (upper) limiting curve, having abscissa u_i^+ (u_i^-) and an ending point, lying on the upper (lower) limiting curve, having abscissa u_j^+ (u_j^-), with $u_i^+=u_j^+-2u_0$ ($u_i^-=u_j^-+2u_0$).

In the generic loading case, $z=c^+$ when $u_i^+\leq u<u_j^+$, and $z=c_u$ when $u>u_j^+$, whereas, in the generic unloading case, $z=c^-$ when $u_j^-<u\leq u_i^-$, and $z=c_l$ when $u<u_j^-$.

Specifically, in this work, the expressions of the upper c_u and lower c_l limiting curves are:

$$c_u=\bar{f}, \tag{4}$$

$$c_l=-\bar{f}, \tag{5}$$

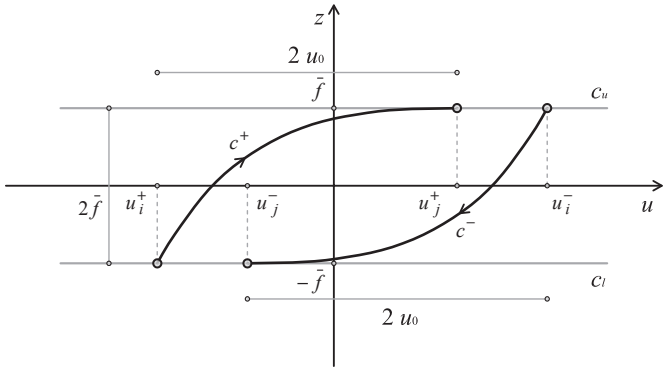

Figure 3: Curves c_u, c_l, c^+, and c^- defining the dimensionless hysteretic variable $z(u)$.

whereas, the ones of the generic loading c^+ and unloading c^- curves are:

$$c^+\left(u, u_j^+\right) = k_a \left[\frac{\left(1 + u - u_j^+ + 2u_0\right)^{(1-\alpha)}}{1-\alpha} - \frac{(1+2u_0)^{(1-\alpha)}}{1-\alpha} \right] + \bar{f}, \tag{6}$$

$$c^-\left(u, u_j^-\right) = k_a \left[\frac{\left(1 - u + u_j^- + 2u_0\right)^{(1-\alpha)}}{\alpha-1} - \frac{(1+2u_0)^{(1-\alpha)}}{\alpha-1} \right] - \bar{f}, \tag{7}$$

where k_a and α are model parameters to be calibrated from experimental tests, whereas u_0 and $\bar{f}$ are two internal model parameters that can be expressed as a function of k_a and α. In particular, $k_a > 0$, $\alpha > 0$, $\alpha \neq 1$, $u_0 > 0$, and $\bar{f} > 0$.

The internal model parameters u_0 and $\bar{f}$ can be evaluated as follows:

$$u_0 = \frac{1}{2} \left[\left(\frac{k_a}{\delta_k} \right)^{\frac{1}{\alpha}} - 1 \right], \tag{8}$$

$$\bar{f} = \frac{k_a}{2} \left[\frac{(1+2u_0)^{(1-\alpha)} - 1}{1-\alpha} \right], \tag{9}$$

where δ_k may be set equal to 10^{-20}, as explained in [13, 14].

Finally, for the generic loading case, the expression of the history variable is:

$$u_j^+ = 1 + u_P + 2u_0 - \left\{ \frac{1-\alpha}{k_a} \left[f_P - \bar{f} + k_a \frac{(1+2u_0)^{(1-\alpha)}}{1-\alpha} \right] \right\}^{\left(\frac{1}{1-\alpha}\right)}, \tag{10}$$

whereas, for the generic unloading case, it becomes:

$$u_j^- = -1 + u_P - 2u_0 + \left\{ \frac{\alpha-1}{k_a} \left[f_P + \bar{f} + k_a \frac{(1+2u_0)^{(1-\alpha)}}{\alpha-1} \right] \right\}^{\left(\frac{1}{1-\alpha}\right)}, \tag{11}$$

where (u_P,f_P) are the coordinates of the initial point P of the generic loading or unloading curve.

Note that, in order to have $max\left\{|z(u)|\right\} = 1$, the parameters k_a and α need to be selected so that Equation (9) gives a unit value of $\bar{f}$.

1. Initial settings.
1.1 Set the model parameters: N, R, μ_{max}, μ_{min}, a, k_a, and α.
1.2 Compute the internal model parameters: $u_0 = \frac{1}{2}\left[\left(\frac{k_a}{\bar{\delta}_k}\right)^{\frac{1}{\alpha}} - 1\right]$ and $\bar{f} = \frac{k_a}{2}\left[\frac{(1+2u_0)^{(1-\alpha)}-1}{1-\alpha}\right]$, with $\delta_k = 10^{-20}$.
2. Calculations at each time step.
2.1 If $s_t s_{t-\Delta t} < 0$, update the history variable: $u_j = u_{t-\Delta t} + s_t\,(1+2u_0) - s_t\left\{\frac{s_t(1-\alpha)}{k_a}\left[z_{t-\Delta t} - s_t\bar{f} + k_a\frac{(1+2u_0)^{(1-\alpha)}}{s_t(1-\alpha)}\right]\right\}^{\left(\frac{1}{1-\alpha}\right)}$.
2.2 Evaluate the dimensionless hysteretic variable at time t: if $u_j s_t - 2u_0 \leq u_t s_t < u_j s_t$: $z_t = k_a\left[\frac{(1+s_t u_t - s_t u_j + 2u_0)^{(1-\alpha)}}{s_t(1-\alpha)} - \frac{(1+2u_0)^{(1-\alpha)}}{s_t(1-\alpha)}\right] + s_t\bar{f}$, otherwise: $z_t = s_t\bar{f}$.
2.3 Compute the kinetic friction coefficient at time t: $\mu_t = \mu_{max} - (\mu_{max} - \mu_{min})\,e^{-a\lvert\dot{u}_t\rvert}$.
2.4 Evaluate the restoring force of the sliding bearing at time t: $f_t = \frac{N}{R}u_t + \mu_t N z_t$.

Table 1: Proposed hysteretic model algorithm.

3.2 Computer Implementation

To allow for an easy computer implementation, Table 1 presents a schematic flowchart of the proposed hysteretic model. To this end, we suppose that a sliding bearing is subjected to a given transverse displacement history and that a displacement-driven solution scheme has been adopted. Because of these assumptions, the displacements $u_{t-\Delta t}$ and u_t, the velocities $\dot{u}_{t-\Delta t}$ and $\dot{u}_t$, as well as the restoring force $f_{t-\Delta t}$ are known over a time step Δt, and the restoring force f_t has to be evaluated.

The implementation scheme of the proposed hysteretic model, summarized in Table 1, is composed of two parts. In the first one, called *Initial settings*, the model parameters, that is, N, R, μ_{max}, μ_{min}, a, k_a, and α are assigned and the internal ones, namely, u_0 and $\bar{f}$, are evaluated. In the second one, called *Calculations at each time step*, the history variable u_j is updated if the sign of the transverse velocity at time t, that is, $s_t = sgn(\dot{u}_t)$, changes with respect to the one at time $t - \Delta t$, that is, $s_{t-\Delta t} = sgn(\dot{u}_{t-\Delta t})$; then, the dimensionless hysteretic variable z_t is computed by using the expression of the generic loading/unloading curve if $u_j s_t - 2u_0 \leq u_t s_t < u_j s_t$; otherwise, it is computed by adopting the expression of the upper/lower limiting curve. Finally, after updating the value of the kinetic friction coefficient μ_t, the restoring force of the sliding bearing f_t is evaluated.

4 VERIFICATION OF THE PROPOSED MODEL

This section presents the validation of the Proposed Hysteretic Model (PHM), described in Section 3. Specifically, numerical accuracy and computational efficiency of the proposed model are assessed by performing Nonlinear Time History Analyses (NLTHAs) on a base-isolated rigid block and comparing the results obtained by modeling the restoring force of each sliding bearing on the basis of the PHM with those obtained by using the model developed by Mokha et al. [10], given by Equations (1)-(3) and referred to as the Mokha Hysteretic Model (MHM) for simplicity.

4.1 Analyzed Mechanical System

Figure 4 illustrates the analyzed mechanical system that consists of a rigid block isolated by two FPBs placed between a shaking table and the rigid block.

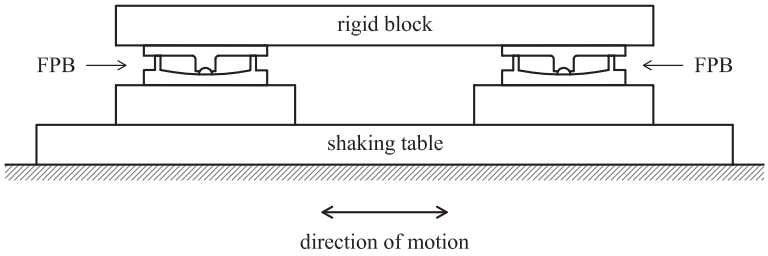

Figure 4: Mechanical system adopted for the numerical verification.

The motion of such a system is described by the following equation:

$$m\ddot{u} + 2c\dot{u} + 2f(u, \dot{u}) = p(t), \tag{12}$$

where m denotes the rigid block mass, c the viscous damping coefficient of each bearing, u, $\dot{u}$, and $\ddot{u}$ the mechanical system displacement, velocity, and acceleration relative to the ground, respectively, f the restoring force of each FPB, and p the external force depending upon time t.

If the mechanical system is subjected to an earthquake excitation, p represents the effective earthquake force, that is, a force acting opposite to the acceleration and equal to mass m times the ground acceleration $\ddot{u}_g$. Thus, Equation (12) is replaced by:

$$m\ddot{u} + 2c\dot{u} + 2f(u, \dot{u}) = -m\ddot{u}_g(t). \tag{13}$$

The rigid block has a mass of 11685.94 $\mathrm{Ns^2m^{-1}}$, whereas the two FPBs, characterized by negligible mass and viscous damping coefficient, have the same properties as the one tested by Mokha et al. [10]. Their nonlinear behavior is simulated by using the hysteretic models parameters listed in Table 2.

4.2 Applied External Forces

The nonlinear dynamic response of the mechanical system is evaluated for two different external forces, namely, a harmonic force and an earthquake force.

The harmonic force, shown in Figure 5a, is a sinusoidal force characterized by an amplitude p_0 that increases linearly with time from 0 to 10^4 N, a forcing frequency $\omega_p = 2\pi$ rad/s, and a time duration $t_d = 10$ s.

MHM	N [N]	R [m]	μ_{max}	μ_{min}	a [s/m]	Y [m]	A	β	γ	n
	57300	0.247	0.075	0.040	43.30	0.0001	1	0.1	0.9	1.1
PHM	N [N]	R [m]	μ_{max}	μ_{min}	a [s/m]	k_a [m^{-1}]	α			
	57300	0.247	0.075	0.040	43.30	15500	7750			

Table 2: Hysteretic models parameters.

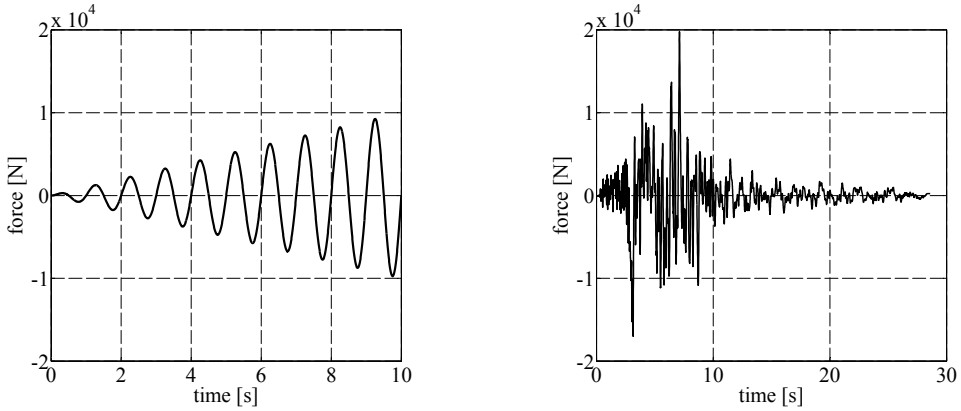

(a) (b)

Figure 5: Applied external forces: harmonic (a) and earthquake force (b).

The earthquake force, shown in Figure 5b, is evaluated by adopting the SN component of horizontal ground acceleration recorded at the Jensen Filter Plant station during the Northridge earthquake of January 17, 1994. The original ground acceleration record, having time step equal to 0.005 s, has been scaled by a factor of 1/3 in order to reach a peak mechanical system displacement, relative to the ground, that is close to the maximum displacement attained by the FPB during the experimental tests conducted by Mokha et al. [10].

4.3 Results of the Nonlinear Time History Analyses

In this subsection, the results of some numerical simulations are presented to assess the numerical accuracy and the computational efficiency of the PHM.

The equation of motion, given by Equation (12) or (13), according to the type of applied external force, has been numerically solved by employing a widely used explicit time integration method, that is, the central difference method [15, 16], and adopting a time step of 0.005 s. In addition, the first-order nonlinear ordinary differential equation characterizing the MHM has been numerically solved by adopting the unconditionally stable semi-implicit Runge-Kutta method [17] and using 50 steps. The numerical time integration algorithm as well as the hysteretic models have been implemented in MATLAB and run on a computer having an Intel®Core™i7-4700MQ processor and a CPU at 2.40 GHz with 16 GB of RAM.

Tables 3 and 4 present the NLTHAs results obtained for the harmonic and earthquake forces, respectively.

The numerical results confirm the accuracy of the PHM since the maximum and minimum

			$u\,[\mathrm{m}]$		$\dot{u}\,[\mathrm{ms}^{-1}]$		$\ddot{u}\,[\mathrm{ms}^{-2}]$	
	$tct\,[\mathrm{s}]$	$tctp$	max	min	max	min	max	min
MHM	9.55	-	0.0350	-0.0321	0.2078	-0.2255	1.4296	-1.5581
PHM	0.07	0.73%	0.0350	-0.0320	0.2077	-0.2253	1.4286	-1.5573

Table 3: NLTHAs results obtained by applying the harmonic force.

			$u\,[\mathrm{m}]$		$\dot{u}\,[\mathrm{ms}^{-1}]$		$\ddot{u}\,[\mathrm{ms}^{-2}]$	
	$tct\,[\mathrm{s}]$	$tctp$	max	min	max	min	max	min
MHM	27.00	-	0.0218	-0.0345	0.1392	-0.1406	1.6221	-1.1974
PHM	0.22	0.81%	0.0218	-0.0346	0.1391	-0.1408	1.6227	-1.1896

Table 4: NLTHAs results obtained by applying the earthquake force.

values of the relative displacement, velocity, and acceleration of the mechanical system, evaluated by employing the proposed model, are quite close to those predicted by the MHM.

Furthermore, the numerical results also show that the computational burden of the PHM, expressed by the total computational time tct, is significantly smaller than the one characterizing the MHM. Since the parameter tct depends upon the amount of the back-ground process running on the computer, the relevant memory, as well as the CPU speed, a fully objective measure of the computational benefits, associated with the use of the PHM with respect to the MHM, is obtained by normalizing such a parameter as follows:

$$\mathrm{PHM}\ tctp\ [\%] = \frac{\mathrm{PHM}\ tct}{\mathrm{MHM}\ tct} \cdot 100\ . \tag{14}$$

Figures 6, 7, and 8 illustrate, respectively, the time histories of the relative displacement, velocity, and acceleration of the mechanical system, whereas Figure 9 shows the restoring force-displacement hysteresis loops displayed by each FPB. Generally speaking, the comparison between the responses simulated with the PHM and the MHM shows a very good agreement.

5 CONCLUSIONS

We have presented a uniaxial phenomenological model able to simulate the complex hysteretic behavior typically displayed by sliding bearings deforming along one of their transverse directions under the effect of an axial compressive load.

The proposed model allows for the evaluation of the device restoring force taking into account its dependency on the sliding velocity, bearing pressure, and sliding surface conditions. Furthermore, such a model requires the solution of an algebraic equation for the evaluation of the hysteretic variable and can be easily implemented in a computer program.

The numerical accuracy and the computational efficiency of the proposed model have been assessed by performing nonlinear time history analyses on a single degree of freedom mechanical system, for two different external forces, that is, a harmonic force and an earthquake force, and comparing the results of the PHM with those associated with the MHM. Specifically, the following conclusions can be drawn:

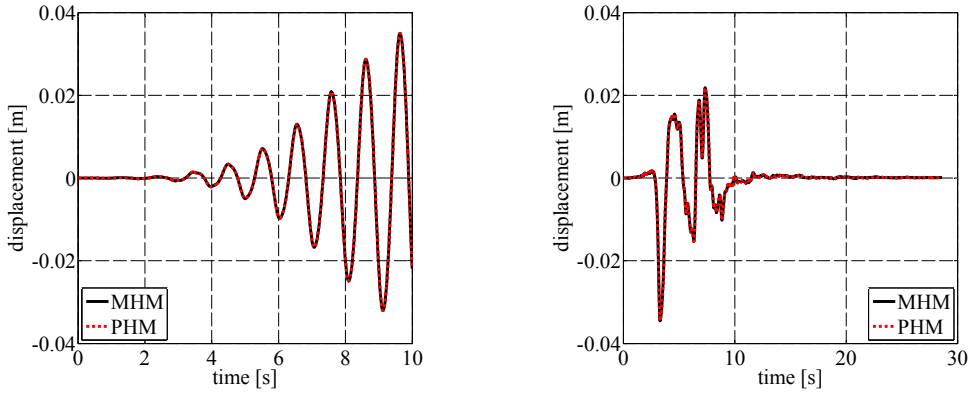

(a) (b)

Figure 6: Relative displacement time history obtained by applying the harmonic (a) and the earthquake force (b).

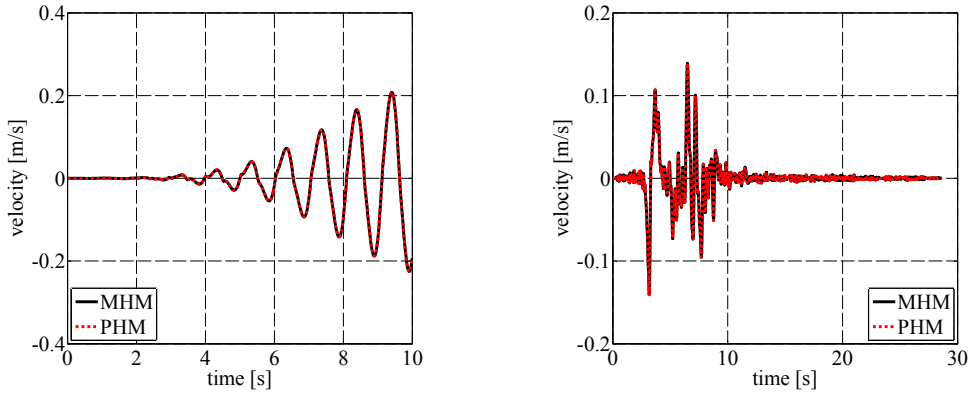

(a) (b)

Figure 7: Relative velocity time history obtained by applying the harmonic (a) and the earthquake force (b).

- the numerical results of the PHM closely match those predicted by the MHM, for both types of external force;
- the total computational time required by the PHM is equal to 0.73% (0.81%), for the harmonic (earthquake) force case, of the one associated with the MHM.

Current research is focusing on the extension of the proposed model to the two-dimensional case through the definition of an interaction domain involving restoring forces. Furthermore, in forthcoming papers, the presented model will be combined with recent strategies to address the nonlinear behavior of framed [18] or shear wall structures [19] in order to analyze base-isolated buildings by exploiting the concept of seismic response envelopes [20].

ACKNOWLEDGMENTS

The present research was supported by the Italian Government, ReLuis 2017 project [AQ DPC/ReLUIS 2014-2018, PR2, Task 2.3] and PRIN 2015 grants [2015JW9NJT-PE8, WP2, Task 2.1], which is gratefully acknowledged by the authors.

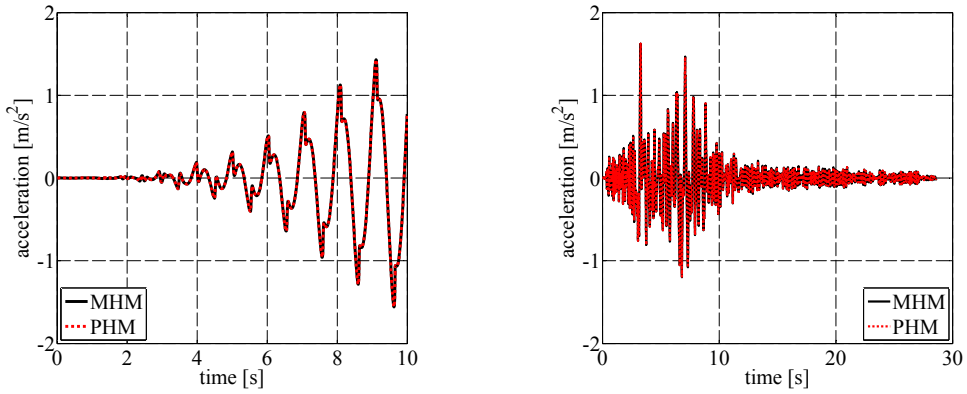

(a) (b)

Figure 8: Relative acceleration time history obtained by applying the harmonic (a) and the earthquake force (b).

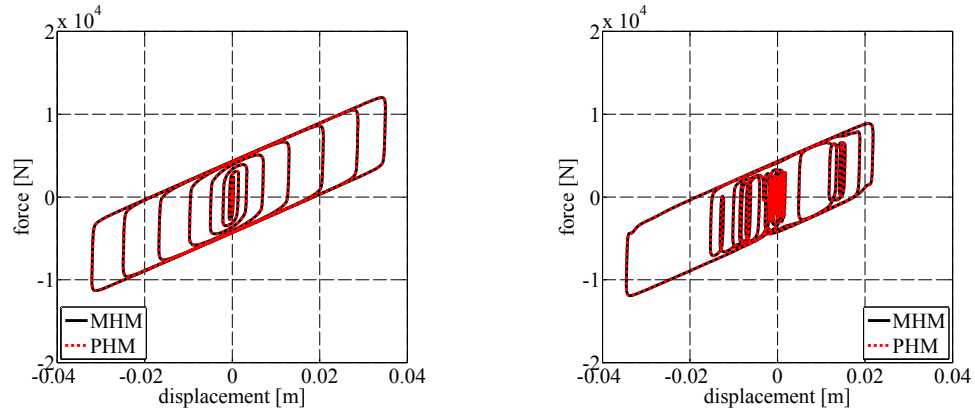

(a) (b)

Figure 9: Hysteresis loops obtained by applying the harmonic (a) and the earthquake force (b).

REFERENCES

[1] D. Losanno, M. Spizzuoco, G. Serino, Optimal design of the seismic protection system for isolated bridges. *Earthquakes and Structures*, **7**(6), 969–999, 2014.

[2] H.A. Hadad, A. Calabrese, S. Strano, G. Serino, A base isolation system for developing countries using discarded tyres filled with elastomeric recycled materials. *Journal of Earthquake Engineering*, **21**(2), 246–266, 2017.

[3] I.E. Madera Sierra, D. Losanno, S. Strano, J. Marulanda, P. Thomson, Development and experimental behavior of HDR seismic isolators for low-rise residential buildings. *Engineering Structures*, **183**(1), 894–906, 2019.

[4] F. Naeim, J.M. Kelly, *Design of seismic isolated structures: from theory to practice*. John Wiley and Sons Inc, 1999.

[5] N. Vaiana, M. Spizzuoco, G. Serino, Wire rope isolators for seismically base-isolated lightweight structures: experimental characterization and mathematical modeling. *Engineering Structures*, **140**(1), 498–514, 2017.

[6] M.C. Constantinou, A.S. Whittaker, Y. Kalpakidis, D.M. Fenz, G.P. Warn, *Performance of seismic isolation hardware under service and seismic loading*. Report No. MCEER-07-0012, State University of New York, Buffalo, NY, USA, 2007.

[7] A. Mokha, M.C. Constantinou, A.M. Reinhorn, Teflon bearings in base isolation. I: Testing. *Journal of Structural Engineering*, **116**(2), 438–454, 1990.

[8] M.C. Constantinou, A. Mokha, A.M. Reinhorn, Teflon bearings in base isolation. II: Modeling. *Journal of Structural Engineering*, **116**(2), 455–474, 1990.

[9] P.C. Tsopelas, P.C. Roussis, M.C. Constantinou, R. Buchanan, A.M. Reinhorn, *3D-BASIS-ME-MB: Computer program for nonlinear dynamic analysis of seismically isolated structures*. Report No. MCEER-05-0009, State University of New York, Buffalo, NY, USA, 2005.

[10] A. Mokha, M.C. Constantinou, A.M. Reinhorn, V.A. Zayas, Experimental study of friction-pendulum isolation system. *Journal of Structural Engineering*, **117**(4), 1201–1217, 1991.

[11] R. Bouc, Modele mathematique d'hysteresis. *Acustica*, **24**(1), 16–25, 1971.

[12] Y.K. Wen, Method for random vibration of hysteretic systems. *Journal of the Engineering Mechanics Division*, **102**(2), 249–263, 1976.

[13] N. Vaiana, S. Sessa, F. Marmo, L. Rosati, A class of uniaxial phenomenological models for simulating hysteretic phenomena in rate-independent mechanical systems and materials. *Nonlinear Dynamics*, **93**(3), 1647–1669, 2018.

[14] N. Vaiana, S. Sessa, F. Marmo, L. Rosati, An accurate and computationally efficient uniaxial phenomenological model for steel and fiber reinforced elastomeric bearings. *Composite Structures*, **211**(1), 196–212, 2019.

[15] K-J. Bathe, *Finite element procedures*. Prentice Hall, 1996.

[16] F. Greco, R. Luciano, G. Serino, N. Vaiana, A mixed explicit-implicit time integration approach for nonlinear analysis of base-isolated structures. *Annals of Solid and Structural Mechanics*, **10**(1), 17–29, 2018.

[17] H.H. Rosenbrock, Some general implicit processes for the numerical solution of differential equations. *The Computer Journal*, **5**(4), 329–330, 1963.

[18] F. Marmo, L. Rosati, The fiber-free approach in the evaluation of the tangent stiffness matrix for elastoplastic uniaxial constitutive laws. *International Journal for Numerical Methods in Engineering*, **94**(9), 868–894, 2013.

[19] N. Valoroso, F. Marmo, S. Sessa, A novel shell element for nonlinear pushover analysis of reinforced concrete shear walls. *Bulletin of Earthquake Engineering*, **13**(8), 2367–2388, 2015.

[20] S. Sessa, F. Marmo, N. Vaiana, L. Rosati, A computational strategy for Eurocode 8 - compliant analyses of reinforced concrete structures by seismic envelopes. *Journal of Earthquake Engineering*, 1–34, 2018. https://doi.org/10.1080/13632469.2018.1551161